Optics and Laser Technology 117 (2019) 272–279

Contents lists available at ScienceDirect

Optics and Laser Technology

journal homepage: www.elsevier.com/locate/optlastec

Full length article

Conjugates of thermally stable phthalocyanine J-type dimers with single-walled carbon nanotubes for enhanced optical limiting applications

Mikhail S. Savelyev[a,b,*], Alexander Yu. Gerasimenko[a,b], Vitaly M. Podgaetskii[a], Sergey A. Tereshchenko[a], Sergey V. Selishchev[a], Alexander Yu. Tolbin[c]

[a] National Research University of Electronic Technology, 124498 Zelenograd, Moscow, Russian Federation
[b] I.M. Sechenov First Moscow State Medical University, 119991 Moscow, Russian Federation
[c] Institute of Physiologically Active Compounds, Russian Academy of Sciences, 142432 Chernogolovka, Moscow Region, Russian Federation

HIGHLIGHTS

- Created liquid and film materials for optical limiters are effective.
- Chemical binding of nanotubes and phthalocyanines forms conjugates.
- The presence of conjugates in materials increases non-linear absorption.
- The dependence of the absorption on the intensity has a threshold character.
- Nanosecond pulses are sharply attenuated, exceeding the threshold intensity.

ARTICLE INFO

Keywords:
Optical limiting
Nanomaterials
Carbon nanotubes
Nonlinear optical properties
phthalocyanine J-type dimers

ABSTRACT

The widespread application of laser devices requires development of new protections against light pulses of high intensity. This problem is relevant because of the danger of hitting the civil aviation pilots with bright and powerful radiation originating from the laser sources which are widely used in the everyday life. Therefore, this work is devoted to continuing our research on a new class of macroheterocyclic compounds – thermally and chemically stable J-type phthalocyanine dimers as potential nonlinear absorbers for optical limiting technology. The dimeric complexes of magnesium (**1a**) and zinc (**1b**) were covalently bonded to single-walled carbon nanotubes (SWCNTs) to improve the overall characteristics of the potential optical limiters **2a,b** as compared to the previously studied corresponding dyes in solutions. The conjugates obtained were investigated using atomic force microscopy (AFM), as well as Raman and IR spectroscopy to confirm formation of the covalent binding of phthalocyanine macrocycles with the carbon surface. Open-aperture Z-scan and a fixed limiter location experiments have demonstrated low values of the limiting threshold and high degree of attenuation of the input laser radiation with the pulses duration located in the nanosecond range.

1. Introduction

Continuous development of laser systems leads to the search for effective means of protection, *i.e.* optical limiters, due to the negative impact of intense radiation on the environment, as well as the eyes and electronic optical sensors [1]. Development of optical limiters is based on the creation of nonlinear absorbers represented as the organic and inorganic materials, whose transmittance decreases sharply after exceeding certain critical energy (limiting threshold) due to the nonlinear optical (NLO) processes [2,3]. A number of demands are put forward to the materials for optical limiters. In particular, nonlinear absorbers should have a high linear transmittance for the low-intensity radiation in a wide range of the light range, as well as a high attenuation coefficient of laser radiation and a short switching-on time (near the transition from linear to nonlinear transmittance). In addition, the absorbing materials should not modify the transmitted radiation, and their design should be simple and reliable with the low production costs [4].

One of the most promising materials that satisfy the listed requirements are the phthalocyanines, which are represented as 18 π-conjugated macroheterocyclic compounds. They have a high radiation resistance, pronounced and easily tunable NLO properties, which are

* Corresponding author.
E-mail addresses: savelyev@bms.zone (M.S. Savelyev), tolbin@ipac.ac.ru (A.Y. Tolbin).

https://doi.org/10.1016/j.optlastec.2019.04.036
Received 15 November 2018; Received in revised form 7 March 2019; Accepted 19 April 2019

controlled by chemical modification of their structure [5–10]. However, conjugation of phthalocyanines with various inorganic nanomaterials, such as graphenes and their oxides [11–13], metal nanoparticles [14] and quantum dots [15], as well as the carbon nanotubes [3,16] is the most interesting deal due to ability to control, in addition to the NLO properties, also the aggregation behavior, which has an important influence on the specificity of the interaction of multicomponent nonlinear absorbers with the laser radiation.

In the present work, new NLO materials based on the covalent conjugation of thermally stable J-type magnesium and zinc phthalocyanine complexes with single-walled carbon nanotubes (SWCNTs) were created for optical limiting applications. Earlier studies of these dyes in solutions have demonstrated low thresholds (0.03–0.05 J/cm^2) for the laser radiation in the nanosecond mode [9], however the degree of attenuation of the radiation fluxes was not sufficient for the problem to be solved. In turn, the synthesized conjugates showed a significant increase in nonlinear absorption coefficients compared with free dyes, which led to an improvement in the characteristics of new materials for optical limiters, bringing us one step closer to solving a strategically important problem.

2. Experimental

2.1. Materials and methods

For the present investigation, phthalocyanine J-type dimeric complexes of Mg (**1a**) and Zn (**1b**) were synthesized according to the previously developed approach [9,17]. SWCNTs were synthesized by an electric arc method on a Ni/Y catalyst, then purified in air and washed with HCl. Carboxylation was carried out in HNO_3/H_2SO_4 to produce SWCNTs-COOH material, followed by washing until neutral. After that, SWCNTs-COOH were treated with $SOCl_2$ to modify carboxylic groups (SWCNTs-COCl material), and conjugates **2a,b** were prepared according to the previously developed method [18] from starting dyes **1a,b** (Scheme 1).

The IR spectra were recorded on a Nicolet iS50 Thermo Scientific Fourier-transform spectrometer in the range of 500–4000 cm^{-1} with the resolution of 1 cm^{-1}, using KBr pellets containing starting dyes **1a,b** or conjugates **2a,b** under investigation. Raman spectra were obtained on a LabRAM HR Evolution HORIBA Scientific spectrometer equipped with the semiconductor laser of 633 nm generation wavelength, impact power of 0.5 mW and duration time of 10 s.

The prepared solutions of **1a,b** in tetrahydrofuran (THF) and aqueous dispersed materials **2a,b** revealed the linear transmittance near 70% with a layer thickness of 2 mm according to the UV/Vis/NIR spectroscopy (Fig. 1).

AFM images were obtained using Icon Brucker atomic force microscope with silicon cantilever in tapping mode at 210 kHz. Dispersion droplets of **2a,b** were placed to a smooth silicon plate for microelectronics by spin coating method and dried in a clean chamber at room temperature for 24 h.

Polymeric films were prepared by simple dispersion of the components – conjugates **2a,b** and polymethylmethacrylate (PMMA) – in THF, followed by evaporation of the solvent *in vacuo*. The thickness of the films did not exceed 1 mm. These films can easily be attached to various surfaces and fixed in the optical device holder.

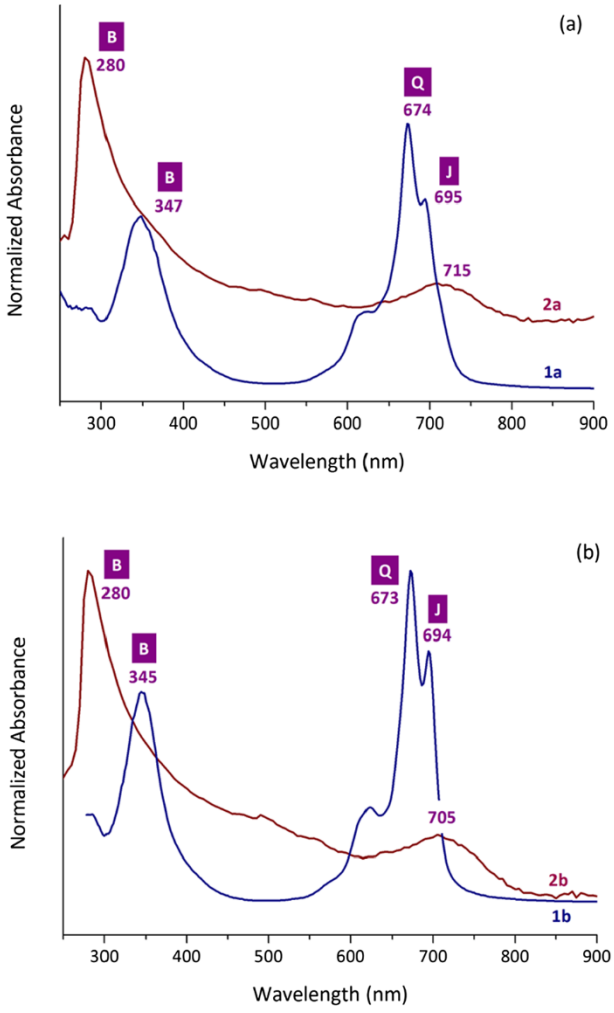

Fig. 1. UV/Vis/NIR of **1a,b** in THF solutions and aqueous dispersions of **2a,b** at 70% linear transmittance (532 nm wavelength and optical pathlength of 2 mm).

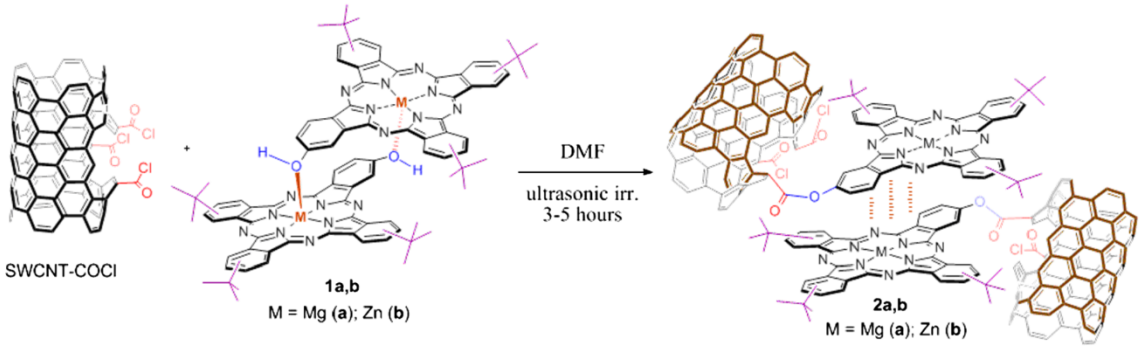

Scheme 1. Synthesis of conjugates of phthalocyanine J-dimers **1a,b** with SWCNTs: a nucleophilic reaction to produce ester bonds for the covalent linkage of the dyes with the carbon surface. Vertical broken lines show π–π- interactions in **2a,b** between the macrocycles, and they are responsible for the stability of the dimeric structures.

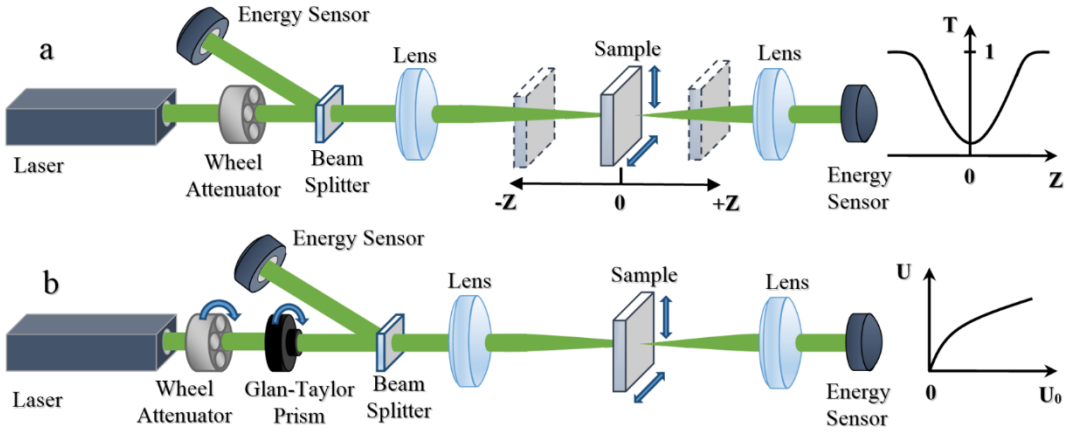

Fig. 2. Graphical representation of the open-aperture Z-scan (a) and fixed sample location (b) experiments. The right charts show a typical kind of the curves for each of the experiment.

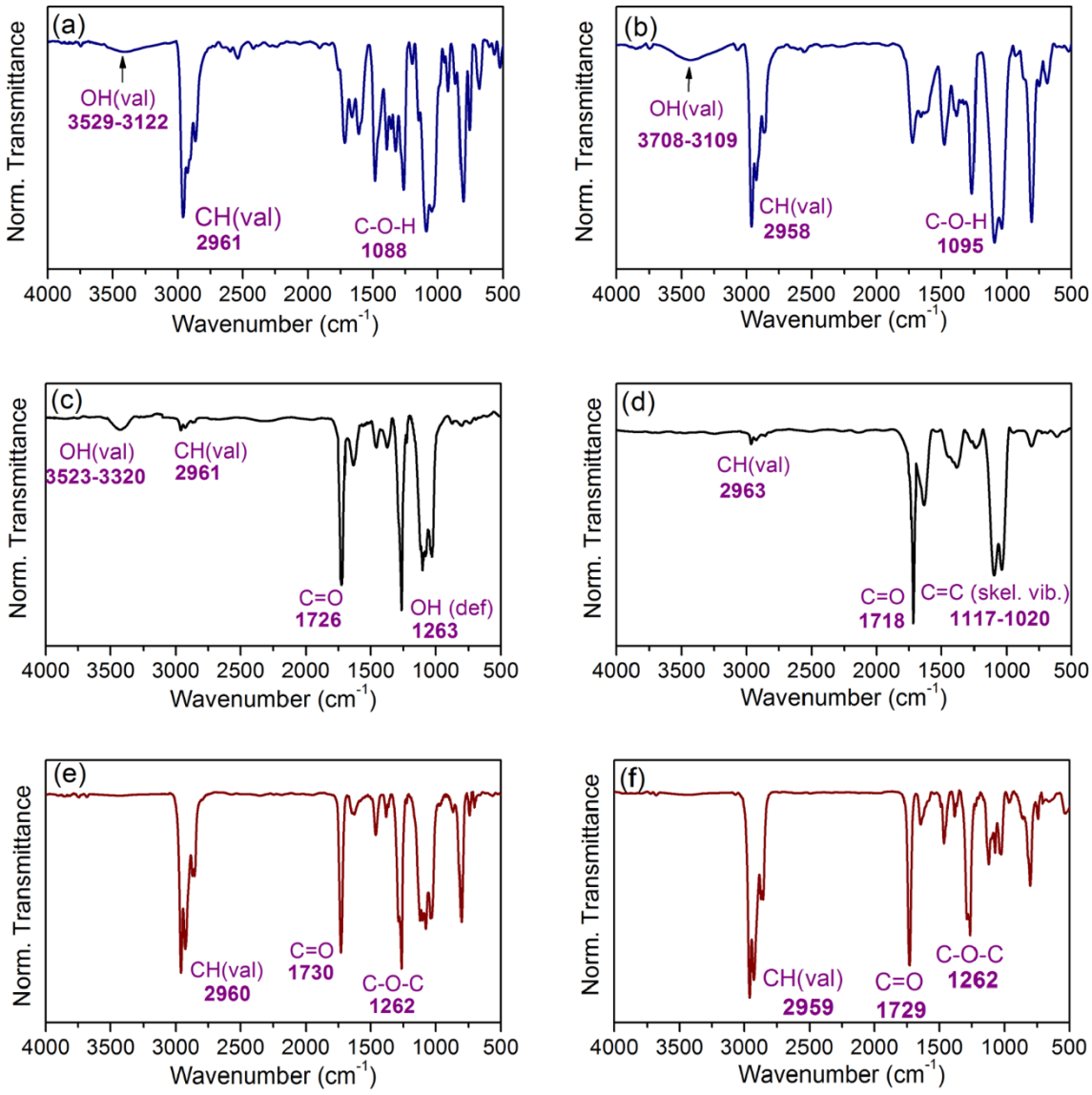

Fig. 3. Fourier transform IR spectra of starting J-dimeric complexes **1a,b** (a, b), carboxylated (c) and acid chloride modified (d) SWCNTs, and conjugates **2a,b** with SWCNTs (e, f).

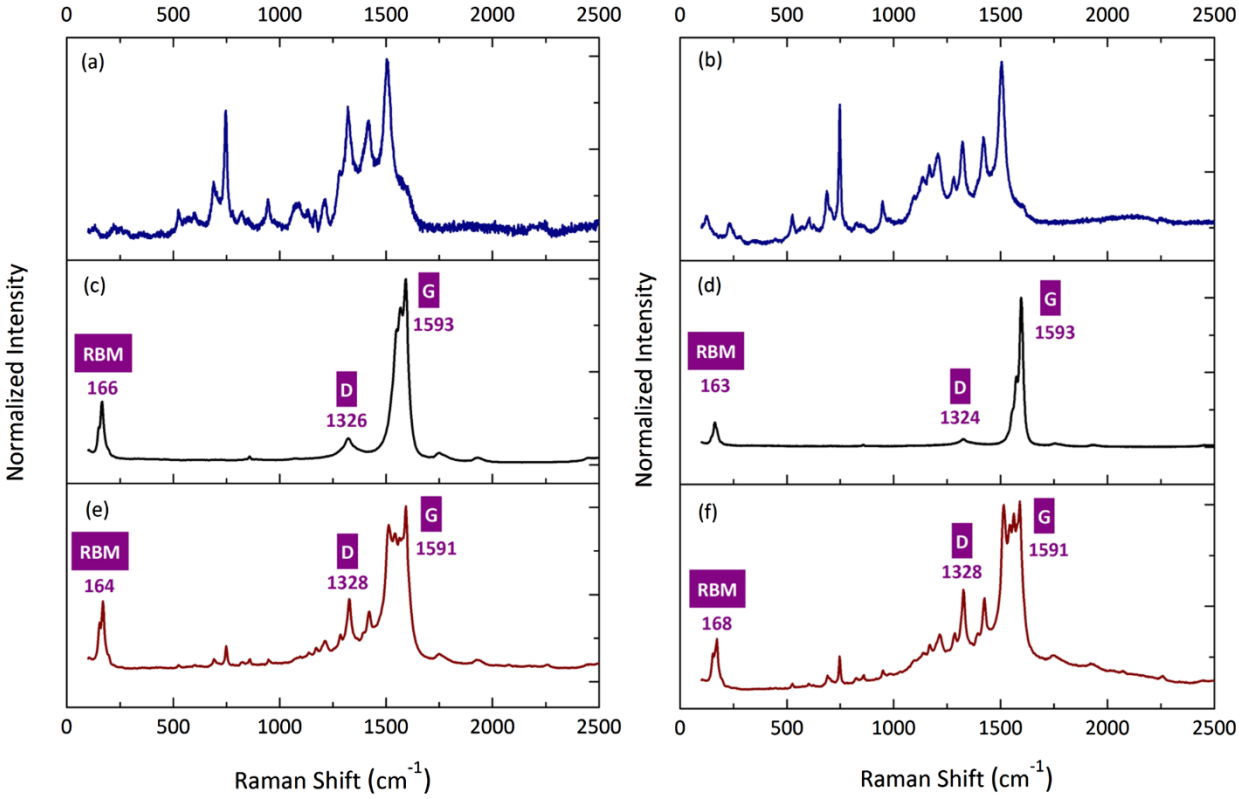

Fig. 4. Raman spectra (633 nm) of starting J-dimeric complexes **1a,b** (a, b), carboxylated (c) and acid chloride modified (d) SWCNTs, and conjugates **2a,b** with SWCNTs (e, f).

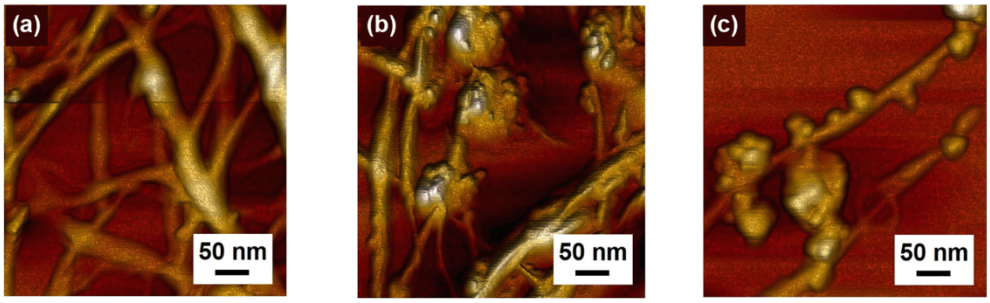

Fig. 5. AFM images of starting SWCNTs (a) and conjugates **2a** (b) and **2b** (c) on a smooth silicon substrate.

2.2. NLO measurements

All NLO experiments were carried out with the use of Nd:YAG laser (LS-2147 Lotis Tii) in Q-swiched mode with pulses duration of 16 ns at a room temperature [9]. The second harmonic generation with the wavelength of 532 nm was applied, which has linear polarization and Gaussian beam profile. During the open-aperture Z-scanning, the energy of single pulses was tuned by the wheel attenuator (Fig. 2a). When the beam had been being passed through the divider, a part of the laser radiation fell onto the sensor to register the input energy. The first lens with a focal length of $f = 20$ cm focused the beam on the sample, which was represented as a solid film or a cuvette with a liquid. The absorber sample had been being moved with a fixed increment, with the transmittance being measured at different points. The sample displacement along the z axis leads to an increase in the energy density due to a decrease in the beam radius as it moves from the lens to its focus ($z = 0$ cm). With further movement, the beam expanded to a second lens with a focal length of $f = 20$ cm. After passing through it, the laser beam had gained the former radius. The output energy was recorded by the sensor.

The experiment with a fixed location of the sample was carried out according to Fig. 2b. A coarse adjustment of the energy of a single pulse was carried out by a wheel attenuator. Its fine adjustment was completed by rotating the Glan-Taylor prism, which is possible due to the linear polarization of the laser beam. The sensor registered different values of the input energy, unlike the Z-scan. The sample was fixed at the point with the minimum radius of the laser beam during irradiation and was displaced to provide hits of the beam into different points.

NLO measurements of solutions and dispersions were studied in a quartz cuvette of 2 mm thickness, and the films were fixed in an optical holder without a substrate and had a thickness of ~ 1 mm. The input U_0 and the output U energies of radiation pulses were recorded by PD10-C and PE9-ES-C sensors (Ophir Photonics).

2.3. Mathematical description

Processing of the experimental data obtained by the methods of a fixed location of the sample and Z-scan with an open aperture was carried out on the basis of the nonlinear radiation transfer equation. The threshold model has allowed us to take into account the transition

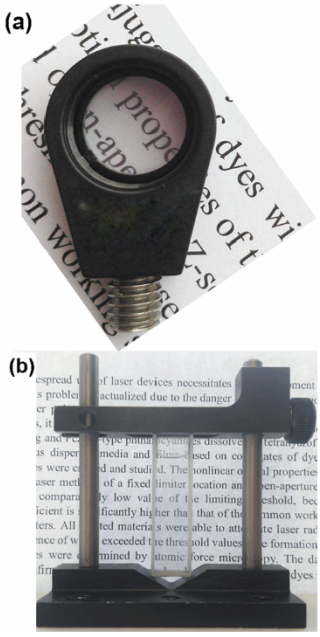

Fig. 6. The photographic images of samples for optical limiters: PMMA film of **2a** (a) and (b) aqueous dispersion of **2b**.

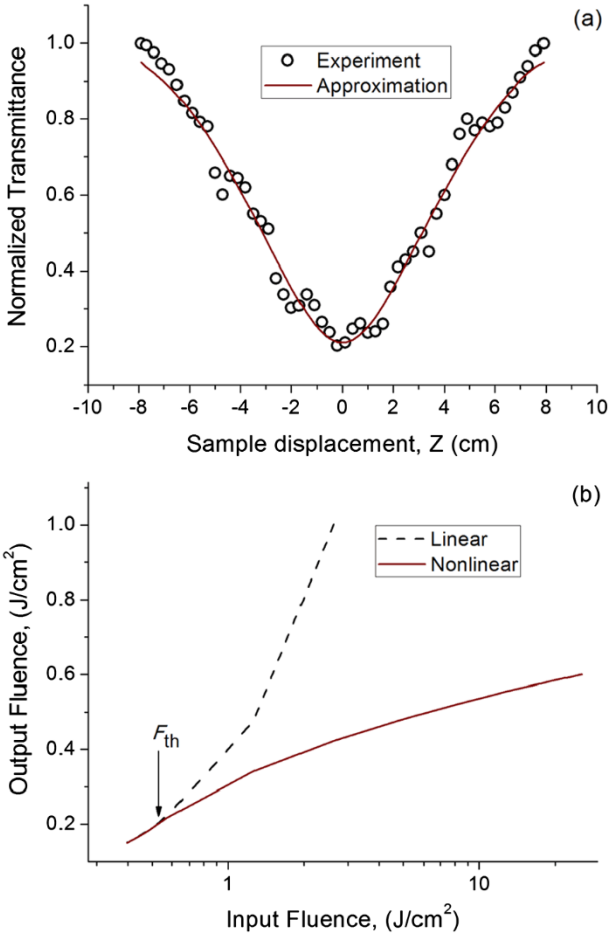

Fig. 7. Z-scan (a) and the fluence output (b) for the optical limiter based on PMMA film of conjugate **2a**. The input fluence is represented in log10 scale to show a deviation from linearity.

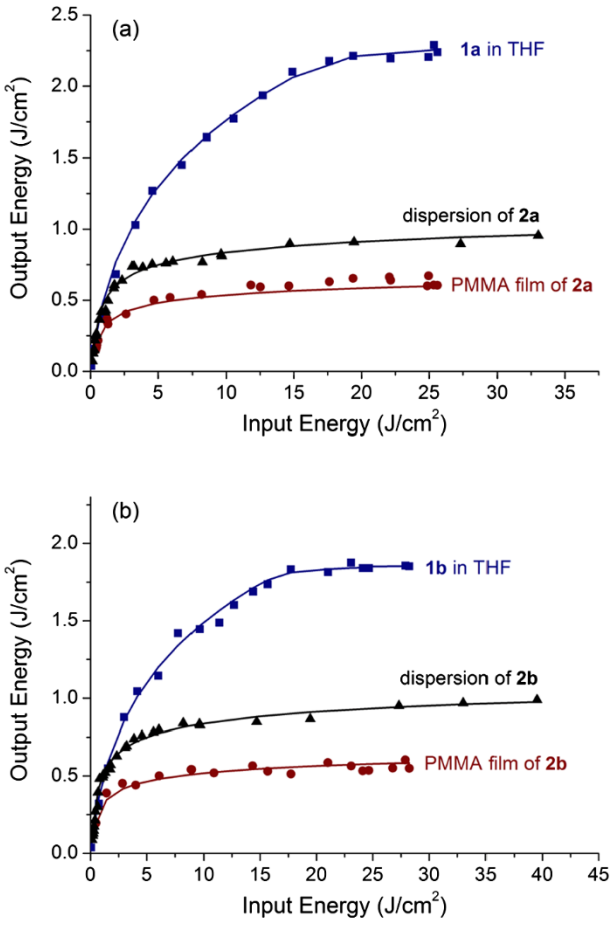

Fig. 8. Energy output for the optical limiters based on conjugates **2a,b** in comparison with corresponding free dyes **1a,b** in THF. The linear transmittance was *ca.* 70% at 532 nm wavelength.

from linear to nonlinear processes [19]. However, in the case of a change in the thickness of the optical layer, the question arises about the maximum allowable value of this parameter, at which this method gives reliable result. As a measure of the permissible thickness of the optical layer, it is convenient to use the Rayleigh length, which characterizes the distance from the waist of the focused laser beam to the point on the axis, where the radius of the laser beam increases by √2 times. With a thickness exceeding this parameter, the energy density significantly changes within the sample that does not allow obtaining reliable data. The Rayleigh length can be determined before placing the sample after measuring the value of the initial radius of the laser beam according to the following equation:

$$z_R = \frac{\lambda f^2}{\pi w_1^2}\left(1 + \left(\frac{\lambda f}{\pi w_1^2}\right)^2\right), \tag{1}$$

where w_1 is the radius of the incident beam at level $1/e^2$.

The radius of the beam after passing the lens was determined by the formula:

$$w^2(z) = \frac{\lambda z_R}{\pi}\left(1 + \frac{z^2}{z_R^2}\right), \tag{2}$$

where z is the sample location relative to the lens focus.

Using the open-aperture Z-scan, the dependence of the transmission T on the sample displacement z with respect to the lens focus was determined. The threshold intensity I_{th}, linear α and nonlinear β absorption coefficients of the laser radiation were determined by the threshold dependence of the total absorption coefficient on the intensity [19].

Table 1
Optical limiting properties of phthalocyanine J-dimers **1a,b** and their conjugates **2a,b** with SWCNTs.

Property	Free dyes in THF		Conjugates (aqueous dispersion)		Conjugates (PMMA films)	
	1a	**1b**	**2a**	**2b**	**2a**	**2b**
Incident beam radius(w_1, cm)	0.05	0.05	0.14	0.14	0.06	0.06
Rayleigh length(Z_R, cm)	2.54	2.54	0.37	0.37	1.79	1.79
Thickness(d, cm)	0.2	0.2	0.2	0.2	0.1	0.1
Input pulse energy (U_0,mJ)	0.4	0.4	0.03	0.03	0.2	0.2
Linear absorption coefficient (α, cm^{-1})	1.5	1.5	2.1	2.1	9.7	9.7
Nonlinear absorption coefficient (β, cm GW^{-1})	340	360	850	750	9500	9000
Optical limiting threshold (F_{th}, J cm^{-2})	0.05	0.03	0.75	0.81	1.01	0.96
Dynamic range (DR)	460	830	140	130	100	110
Attenuation coefficient (K)	7	7.8	25	24	44	42

Knowing the values of these characteristics for each absorber, one can determine the energy density immediately after the sample by the formula:

$$F(\rho, z, U_0) = F_0(\rho, z, U_0)\exp(-\alpha d)\frac{2}{\sqrt{\pi}}\left[\frac{\sqrt{\pi}}{2} - \eta(\gamma_{th}-1)\mathrm{ls}_0(0, 1, \sqrt{\ln(\gamma_{th})}) + \frac{\eta(\gamma_{th}-1)}{\gamma_{th}}\left(\frac{\alpha\tau\sqrt{\pi}\gamma_{th}}{\alpha\tau\sqrt{\pi}-\beta F_{th}}\right)^{\frac{\alpha\tau\sqrt{\pi}}{\alpha\tau\sqrt{\pi}-\beta F_{th}}}\mathrm{ls}_0\left(\frac{\beta F_{th}\gamma_{th}}{\alpha\tau\sqrt{\pi}-\beta F_{th}}, \frac{\alpha\tau\sqrt{\pi}}{\alpha\tau\sqrt{\pi}-\beta F_{th}}, \sqrt{\ln(\gamma_{th})}\right) - \frac{\eta(\gamma_{th}-1)\eta(\gamma_{th1}-1)}{\gamma_{th}}\left(\frac{\alpha\tau\sqrt{\pi}\gamma_{th}}{\alpha\tau\sqrt{\pi}-\beta F_{th}}\right)^{\frac{\alpha\tau\sqrt{\pi}}{\alpha\tau\sqrt{\pi}-\beta F_{th}}}\mathrm{ls}_0\left(\frac{\beta F_{th}\gamma_{th}}{\alpha\tau\sqrt{\pi}-\beta F_{th}}, \frac{\alpha\tau\sqrt{\pi}}{\alpha\tau\sqrt{\pi}-\beta F_{th}}, \sqrt{\ln(\gamma_{th1})}\right) + \eta(\gamma_{th}-1)\eta(\gamma_{th1}-1)\exp\left(\frac{\beta F_{th}d}{\tau\sqrt{\pi}}\right)\mathrm{ls}_0\left(\frac{\beta F_{th}\gamma_{th}}{\alpha\tau\sqrt{\pi}-\beta F_{th}}\left(1 - \exp\left[\frac{\beta F_{th}}{\tau\sqrt{\pi}}d - \alpha d\right]\right), 1, \sqrt{\ln(\gamma_{th1})}\right)\right], \quad (3)$$

where ρ is the radius vector in the polar coordinate system, $\gamma_{th} = \frac{2U_0 z_R}{F_{th}\lambda(z_R^2+z^2)}\exp\left(-\frac{2\rho^2\pi z_R}{\lambda(z_R^2+z^2)}\right)$, $\gamma_{th1} = \frac{2U_0 z_R}{F_{th1}\lambda(z_R^2+z^2)}\exp\left(-\frac{2\rho^2\pi z_R}{\lambda(z_R^2+z^2)}\right)$, $F_{th} = I_{th}\tau\sqrt{\pi}$, $F_{th1} = \frac{(\alpha\tau\sqrt{\pi}-\beta F_{th})F_{th}}{\alpha\tau\sqrt{\pi}\exp\left(-\left[\alpha-\beta\frac{F_{th}}{\tau\sqrt{\pi}}\right]d\right)-\beta F_{th}}$, $\mathrm{ls}_0(a, b, c) = \int_0^c\left(\frac{\exp(-r^2)}{1+a\exp(-r^2)}\right)^b dr$.

It is worth noting that, in accordance with this formula, the pulse profile becomes non-Gaussian after passing through the sample. In this case, the incident energy density of the laser radiation can be calculated at any point with the z coordinate after the lens in accordance with the Gauss dependence, taking into account the change in the beam radius (2):

$$F_0(\rho, z, U_0) = \frac{2U_0 z_R}{\lambda(z_R^2+z^2)}\exp\left(-\frac{2\rho^2\pi z_R}{\lambda(z_R^2+z^2)}\right). \quad (4)$$

3. Results

3.1. Synthesis and DFT study

Conjugates **2a,b** were obtained during heterophase reaction between acid chloride modified nanotubes SWCNTs–COCl and J-type phthalocyanine complexes **1a,b** in dimethylformamide (DMF) under ultrasonic irradiation:

On proceeding the reaction, we have being observed the disappearance of the phthalocyanine coloring, which indicated the inclusion of phthalocyanine molecules in the structure of the nanomaterial.

DFT calculations, provided by the time-consuming procedure with the use of PBE functional [20] and cc-pVDZ basis set (PRIRODA package [21]), have revealed the fact of increased macrocyclic slippage in the final conjugate structures on an example of the model corresponded to zinc derivative **2b**. Thus, magnification of the slip angle from 18.9 deg. [9] to 34.7 deg. is attributed to the lack of free space occupied by the carbon nanosurface in the vicinity of hydroxyl groups. At the same time, the dimeric structure remains stable despite an insignificant increase in the distance between the macrocycles in comparison with the starting dimeric structure. In the reality the dimeric molecules appear to occupy the defective space of the nanotubes, geometrically adjusting to it by sliding the macrocycles.

3.2. IR spectroscopy

The IR spectra of starting materials – J-dimers **1a,b** and SWCNTs, as well as the conjugate products (compounds **2a,b**) are presented in Fig. 3. For the initial dyes, two characteristic vibration bands are observed (Fig. 3a and b), corresponding to the stretching vibrations of the O—H bond (near 3500 cm^{-1}) and the presence in the molecules of the C—O—H fragments (near 1090 cm^{-1}), which disappear during the formation of covalent bonds with the nanosurface (Fig. 3e and f). At the same time, the signals from C═O vibrational modes coming from nanotubes are clearly visible in the spectra of conjugates **2a,b**. Additionally, the fact of covalent binding is confirmed by the presence of vibrations from the C—O—C bonds. Note that the modification of carboxylic acid functions in the starting nanotubes (SWCNTs–COOH → SWCNTs–COCl) occurs disappearance of signals related to the stretching and deformation vibrations of the O—H bonds (near 3500 and 1260 cm^{-1} respectively – Fig. 3c and d), which confirms the purity of the experiment.

3.3. Raman spectroscopy

The Raman spectra were obtained in the range of 100–2500 cm^{-1} for starting phthalocyanine J-dimers **1a,b**, SWCNTs and conjugates **2a,b**.

The surface of SWCNTs similarly to the graphene sheet structure consists of sp^2-hybridized carbon atoms. Fig. 4(c)–(f) demonstrate G and D scattering bands which are characteristic of two-dimensional materials. With the destruction of bonds in the carbon material, sp^3-hybridized carbon atoms move outside the graphene plane and being oscillated with the D mode frequency unlike the non-defective material, which oscillates only with the G mode frequency. For this reason, the ratio D/G is considered as the measure of SWCNTs defectiveness [22]. The D/G interrelation for the starting SWCNTs–COOH was found to be 0.116. Treatment of the initial SWCNTs–COOH with thionyl chloride lowers the value of defects of the carbon structure, and subsequent conjugation with the J-dimers **1a,b** results in an increasing in the defectiveness. Thus, for conjugates **2a,b**, the D/G parameter is calculated to be 0.519 and 0.460 respectively, demonstrating the fact of the covalent binding of the dyes to the SWCNTs surface. We should also point out the change in the RBM band position during all modifications.

The RBM band is attributed to the symmetric vibrations of carbon atoms in the radial directions [23], and for the SWCNTs it is possible to estimate the effective diameter referring to the empirical statements [24]. The average diameter of SWCNTs–CO(OH,Cl) and corresponding conjugates **2a,b** was found to be no more than 1.5 nm. This value slightly alters during the chemical processes, further confirming the formation of covalent bonds.

3.4. AFM study

Analysis of the AFM topograms of the original carboxylated nanotubes SWCNTs–COOH showed the nano objects in the form of individual fibers and their bundles, with the diameter being varied from 5 to 65 nm and the length reaching up to 7–8 μm (Fig. 5a). A large number of nanotubes are detected in the form of individual fibers. SWCNTs are evenly distributed on the surface of the substrate. Since the SWCNTs are observed as linear or spindle-shaped formations, this indicates a high degree of structural perfection of the nanomaterial.

Conjugation of SWCNTs with the phthalocyanines leads to a significant change in their structure (Fig. 5), resulting in the appearance of growths separated into small spherical objects. These are nanoclusters, or aggregates of free molecules of the starting phthalocyanines **1a,b**. For the magnesium conjugate **2a** (Fig. 5b), the scale of the nanoclusters do not exceed 20 nm, while for the zinc conjugate **2b** they reach 80 nm. This suggests that zinc J-dimer **1b** aggregates more strongly than its magnesium derivative **1a** under the reaction conditions.

Aggregation of the macrocyclic dyes is responsible for the strong divergence of the calculated diameter of nanotubes (from the Raman spectra) with those determined from AFM micrographs. In addition, the aggregation effect is pronounced in the absorption spectra for **2a,b** (Fig. 1), where the Q bands are broadened and significantly lower than the corresponding B bands, unlike starting dyes **1a,b**.

Thus, we have obtained the covalent conjugates of phthalocyanine J-dimers with the single-walled carbon nanotubes, and an excess of phthalocyanine molecules is retained in the nanomaterial structure in the form of aggregates – nanoclusters. At the same time, the strength of binding seems to be high, since the fact of “leaching” of free dyes was not detected during the NLO experiments.

3.5. Materials for optical limiters

The resulting materials **2a,b** for optical limiters represented as the PMMA films or aqueous dispersions exhibited high transparency in the visible range. They do not distort the geometry or color reproduction of the transmitted images (Fig. 6). Concentration of the nano absorbers did not exceed 0.001 wt%, and the linear transmittance was *ca.* 70% at a wavelength of 532 nm.

High transmittance for low-intensity (non-hazardous) laser radiation is one of the important indicators for materials that have the potential to be used in the optical limiting technology.

3.6. Nonlinear optical properties

Among the series of NLO phenomena that favorably affect the optical limiting, nonlinear absorption is generally considered, being the dominant process along with possible scattering on large particles of nanomaterials [25–27] that promotes thermal processes to enhance the observed NLO response [28,29], especially at high pulse repetition rates [30–32]. It is worth noting that, the change in the wavelength of the laser radiation can lead to a weakening of the joint action of involved processes [33]. Z-scan with an open aperture, although it does not allow to evaluate the contribution of each of the phenomena, but at the same time provides reliable data on the total effect pronounced in the radiation transmittance scale when the sample is being displaced along the propagation axis of this radiation. As an example, Fig. 7 shows the results of NLO experiments – Z-scan with an open aperture and the output characteristic of the optical limiter based on conjugate **2a**. The energy flux density of the output radiation, F, was calculated according to Eqs. (3) and (4). Since nonlinear deviation (Fig. 7b) is already observed in the region of small values of input energy, it is necessary to use mathematical models for its exact localization.

Thus, with the help of the threshold model [19], we calculated the threshold intensity I_{th} and nonlinear absorption coefficient β based on the Z-scan experiment. Then, the output characteristics of the model limiters based on conjugates **2a,b** were calculated in the form of the energy transmitted through the absorber layer as a function of the input energy with a fixed location of the corresponding samples relative to the lens focus. The corresponding experimental values were obtained by measuring the nonlinear transmittance during a smooth change in the energy of the input radiation. The theoretical curves (solid lines in Fig. 8) were calculated for each sample from the already known values of the threshold energy density F_{th}, linear α and nonlinear β absorption coefficients. Fig. 8 shows a good agreement between experimental and theoretical values that confirms the validity of the mathematical model used. The results are summarized in Table 1.

The dynamic ranges (DR) and attenuation coefficients (K) were determined according to the previously described method [9].

4. Discussion

The resulting conjugates of phthalocyanine dyes with carbon nanotubes can be used in optical devices to protect the eyes and light-sensitive elements of optical devices. Our studies have shown that nonlinear absorbers in the form of aqueous dispersions of conjugates **2a,b** decrease the laser radiation energy more strongly, compared to solutions of free dyes **1a,b** in THF. This result can be explained by the contribution of nonlinear scattering due to the appearance of a gaseous phase – air bubbles when a liquid boils [34]. At the same time, one cannot exclude an increase in the absorption of radiation due to an increase in the optical path of the laser beam inside the samples of aqueous dispersions.

The main mechanism that underlies the optical limiting is reverse saturable absorption, induced by multiphoton absorption [9]. But in the case of our nanomaterials, photoinduced electron and energy transfer between dyes **1a,b** and SWCNTs can also be added to this effect and to the effect of nonlinear scattering. Apparently, therefore, we achieved the greatest attenuation of radiation in the case of PMMA films of conjugates **2a,b**. In addition, since the particle size in the films is higher than for dispersions, the scattering will more effectively attenuate the input radiation, giving thin films of optical limiters based on conjugates of phthalocyanine J-dimers with SWCNTs the best qualities. According to data obtained earlier [19], nonlinear effects are more weak for pulses of 7 ns duration in comparison with pulses of 16 ns duration. Therefore, nonlinear effects are probably due to slow thermal processes. Shorter pulses will be lesser attenuated. At the same time, for higher intensity of the laser radiation, the multiphoton absorption will lead to the more strong nonlinear effects.

Thus, we concluded that the joint action of absorption, scattering on large and inhomogeneous particles, and also photoinduced processes increases the nonlinear attenuation of laser radiation in thin films. For all studied absorbers, the use of the threshold model [19] made it possible to accurately approximate the experimental data and calculate the effective parameters of optical limiters (Table 1).

5. Conclusions

In this work, new nanomaterials for optical limiters based on conjugates of J-type magnesium and zinc phthalocyanine complexes with the single-walled carbon nanotubes were created. Covalent attachment was proved by IR/Raman spectra. In particular, the disappearance of the broad band in the region of 3600–3100 cm^{-1} (OH) in the IR spectra of **2a,b** and the appearance of a sharp signal at *ca.* 1730 cm^{-1} (C═O)

indicates the formation of an ester bond. Functionalization leads to an increase in the defectiveness of the nanomaterial structure, which is caused by the phenomenon of aggregation. Thus, AFM images show a significant increase in the number of nanoclusters in the area of functional groups on the SWCNT surface, and the shifting of the RBM band characterizes the change in the effective diameter of the nanotubes.

The optical limiting effect for solutions of free dyes **1a,b** in THF and conjugates **2a,b** in the form of PMMA films and aqueous dispersions at a wavelength of 532 nm has been studied. For 70% linear transmittance, nanomaterials did not distort the color of the transmitted objects, which is a good indicator. However, for conjugates **2a,b**, higher thresholds of optical limiting were found, compared to solutions. The experimental data were approximated by the "threshold" model to show an excellent correlation between experiment and theory. It has been found that thin film samples more effectively attenuate the laser radiation, while they significantly simplify the design of limiters, since can be applied to any glass surface.

The obtained conjugates of J-type phthalocyanine complexes of magnesium and zinc with single-walled carbon nanotubes can be used to protect the eyes and photosensitive elements of optical devices from high-power laser radiation whose duration is not less than 16 ns.

Acknowledgements

This work was provided by the Ministry of Education and Science of the Russian Federation (Agreement 14.578.21.0234 RFMEFI57817X0234). The authors thank the Joint Supercomputer Centre of RAS (www.jscc.ru) for providing computing resources. The studies were performed using MIET Core facilities center "MEMS and electronic components MIET".

References

[1] M.W. Geis, P.J. Bos, V. Liberman, M. Rothschild, Broadband optical switch based on liquid crystal dynamic scattering, Opt. Express 24 (2016) 13812, https://doi.org/10.1364/OE.24.013812.
[2] S.M. O'Flaherty, S.V. Hold, M.J. Cook, T. Torres, Y. Chen, M. Hanack, W.J. Blau, Molecular engineering of peripherally and axially modified phthalocyanines for optical limiting and nonlinear optics, Adv. Mater. 15 (2003) 19–32, https://doi.org/10.1002/adma.200390002.
[3] K. Sanusi, E.K. Amuhaya, T. Nyokong, Enhanced optical limiting behavior of an indium phthalocyanine–single-walled carbon nanotube composite: an investigation of the effects of solvents, J. Phys. Chem. C 118 (2014) 7057–7069, https://doi.org/10.1021/jp501469e.
[4] A.E. Siegman, Nonlinear optical effects: an optical power limiter, Appl. Opt. 1 (1962) 127, https://doi.org/10.1364/AO.1.S1.000127.
[5] J. Chen, T. Zhang, S. Wang, R. Hu, S. Li, J.S. Ma, G. Yang, Intramolecular aggregation and optical limiting properties of triazine-linked mono-, bis- and tris-phthalocyanines, Spectrochim. Acta Part A Mol. Biomol. Spectrosc. 149 (2015) 426–433, https://doi.org/10.1016/j.saa.2015.04.093.
[6] A. Fashina, T. Nyokong, Nonlinear optical response of tetra and mono substituted zinc phthalocyanine complexes, J. Lumin. 167 (2015) 71–79, https://doi.org/10.1016/j.jlumin.2015.06.003.
[7] A. Tuhl, H. Manaa, S. Makhseed, N. Al-Awadi, J. Mathew, H.M. Ibrahim, T. Nyokong, H. Behbehani, Reverse saturation absorption spectra and optical limiting properties of chlorinated tetrasubstituted phthalocyanines containing different metals, Opt. Mater. (Amst) 34 (2012) 1869–1877, https://doi.org/10.1016/j.optmat.2012.05.018.
[8] L. Zhang, L. Wang, Recent research progress on optical limiting property of materials based on phthalocyanine, its derivatives, and carbon nanotubes, J. Mater. Sci. 43 (2008) 5692–5701, https://doi.org/10.1007/s10853-008-2826-4.
[9] A.Y. Tolbin, M.S. Savelyev, A.Y. Gerasimenko, L.G. Tomilova, N.S. Zefirov, Thermally stable J-type phthalocyanine dimers as new non-linear absorbers for low-threshold optical limiters, PCCP 18 (2016), https://doi.org/10.1039/c6cp01862a.
[10] A.Y. Tolbin, L.G. Tomilova, N.S. Zefirov, Non-symmetrically substituted phthalocyanines: synthesis and structure modification, Russ. Chem. Rev. 76 (2007) 681–692, https://doi.org/10.1070/RC2007v076n07ABEH003698.
[11] M. Yadi, R. Karimzadeh, A. Abbasi, Effect of treatment by electrostatic field and 532-nm laser irradiation on optical and thermo-optical properties of graphene oxide colloids, J. Mater. Sci. 52 (2017) 4532–4542, https://doi.org/10.1007/s10853-016-0698-6.
[12] J. Zhu, Y. Li, Y. Chen, J. Wang, B. Zhang, J. Zhang, W.J. Blau, Graphene oxide covalently functionalized with zinc phthalocyanine for broadband optical limiting, Carbon N. Y. 49 (2011) 1900–1905, https://doi.org/10.1016/j.carbon.2011.01.014.
[13] X. Zhao, X.-Q. Yan, Q. Ma, J. Yao, X.-L. Zhang, Z.-B. Liu, J.-G. Tian, Nonlinear optical and optical limiting properties of graphene hybrids covalently functionalized by phthalocyanine, Chem. Phys. Lett. 577 (2013) 62–67, https://doi.org/10.1016/j.cplett.2013.04.023.
[14] D. Tan, X. Liu, Y. Dai, G. Ma, M. Meunier, J. Qiu, A universal photochemical approach to ultra-small, well-dispersed nanoparticle/reduced graphene oxide hybrids with enhanced nonlinear optical properties, Adv. Opt. Mater. 3 (2015) 836–841, https://doi.org/10.1002/adom.201400560.
[15] K. Sanusi, S. Khene, T. Nyokong, Enhanced optical limiting performance in phthalocyanine-quantum dot nanocomposites by free-carrier absorption mechanism, Opt. Mater. (Amst) 37 (2014) 572–582, https://doi.org/10.1016/j.optmat.2014.07.024.
[16] N. He, Y. Chen, J. Bai, J. Wang, W.J. Blau, J. Zhu, Preparation and optical limiting properties of multiwalled carbon nanotubes with π-conjugated metal-free phthalocyanine moieties, J. Phys. Chem. C 113 (2009) 13029–13035, https://doi.org/10.1021/jp9006813.
[17] A.Y. Tolbin, V.E. Pushkarev, I.O. Balashova, A.V. Dzuban, P.A. Tarakanov, S.A. Trashin, L.G. Tomilova, N.S. Zefirov, A highly stable double-coordinated 2-hydroxy-tri(tert-butyl)-substituted zinc phthalocyanine dimer: synthesis, spectral study, thermal stability and electrochemical properties, New J. Chem. 38 (2014) 5825–5831, https://doi.org/10.1039/C4NJ00692E.
[18] A.Y. Tolbin, V.N. Khabashesku, L.G. Tomilova, Synthesis of phthalocyanine tert-butyl ligand conjugates with fluorinecontaining single-walled carbon nanotubes having mobile ether bonds, Mendeleev Commun. 22 (2012) 59–61, https://doi.org/10.1016/j.mencom.2012.03.001.
[19] S.A. Tereshchenko, M.S. Savelyev, V.M. Podgaetsky, A.Y. Gerasimenko, S.V. Selishchev, Nonlinear threshold effect in the Z-scan method of characterizing limiters for high-intensity laser light, J. Appl. Phys. 120 (2016), https://doi.org/10.1063/1.4962199.
[20] M. Ernzerhof, G.E. Scuseria, Assessment of the Perdew–Burke–Ernzerhof exchange-correlation functional, J. Chem. Phys. 110 (1999) 5029–5036, https://doi.org/10.1063/1.478401.
[21] D.N. Laikov, A new class of atomic basis functions for accurate electronic structure calculations of molecules, Chem. Phys. Lett. 416 (2005) 116–120, https://doi.org/10.1016/j.cplett.2005.09.046.
[22] H.F. Bettinger, Carbon nanotubes basic concepts and physical properties. By S. Reich, C. Thomsen, J. Maultzsch, ChemPhysChem 5 (2004) 1914–1915, https://doi.org/10.1002/cphc.200400387.
[23] M.S. Dresselhaus, G. Dresselhaus, R. Saito, A. Jorio, Raman spectroscopy of carbon nanotubes, Phys. Rep. 409 (2005) 47–99, https://doi.org/10.1016/j.physrep.2004.10.006.
[24] H. Wang, L. Wang, Y. Wang, X. Cao, M. Feng, Q. Jin, D. Ding, G. Lan, Vibrational properties of single-wall BC3 nanotubes, J. Phys. Chem. Solids 70 (2009) 8–14, https://doi.org/10.1016/j.jpcs.2008.08.010.
[25] S.J. Varma, J. Kumar, Y. Liu, K. Layne, J. Wu, C. Liang, Y. Nakanishi, A. Aliyan, W. Yang, P.M. Ajayan, J. Thomas, 2D TiS 2 layers: a superior nonlinear optical limiting material, Adv. Opt. Mater. 5 (2017) 1700713, https://doi.org/10.1002/adom.201700713.
[26] J.E. Riggs, D.B. Walker, D.L. Carroll, Y.-P. Sun, Optical limiting properties of suspended and solubilized carbon nanotubes, J. Phys. Chem. B 104 (2000) 7071–7076, https://doi.org/10.1021/jp0011591.
[27] Y. Chen, Y. Lin, Y. Liu, J. Doyle, N. He, X. Zhuang, J. Bai, W.J. Blau, Carbon nanotube-based functional materials for optical limiting, J. Nanosci. Nanotechnol. 7 (2007) 1268–1283, https://doi.org/10.1166/jnn.2007.308.
[28] A.V. Venediktova, A.Y. Vlasov, E.D. Obraztsova, D.A. Videnichev, I.M. Kislyakov, E.P. Sokolova, Stability and optical limiting properties of a single wall carbon nanotubes dispersion in a binary water-glycerol solvent, Appl. Phys. Lett. 100 (2012) 251903, https://doi.org/10.1063/1.4729790.
[29] L. Polavarapu, N. Venkatram, W. Ji, Q.-H. Xu, Optical-limiting properties of oleylamine-capped gold nanoparticles for both femtosecond and nanosecond laser pulses, ACS Appl. Mater. Interfaces 1 (2009) 2298–2303, https://doi.org/10.1021/am900442u.
[30] D.N. Christodoulides, I.C. Khoo, G.J. Salamo, G.I. Stegeman, E.W. Van Stryland, Nonlinear refraction and absorption: mechanisms and magnitudes, Adv. Opt. Photonics 2 (2010) 60, https://doi.org/10.1364/AOP.2.000060.
[31] J. Huang, N. Dong, S. Zhang, Z. Sun, W. Zhang, J. Wang, Nonlinear absorption induced transparency and optical limiting of black phosphorus nanosheets, ACS Photon. 4 (2017) 3063–3070, https://doi.org/10.1021/acsphotonics.7b00598.
[32] Z. Xu, Q. Guo, C. Liu, Z. Ma, X. Liu, J. Qiu, Linear and nonlinear optical characteristics of Te nanoparticles-doped germanate glasses, Appl. Phys. B 122 (2016) 259, https://doi.org/10.1007/s00340-016-6534-5.
[33] Y. Zhang, Y. Song, Y. Gan, M. Feng, H. Zhan, Broadband nonlinear optical and optical limiting effects of partially unzipped carbon nanotubes, J. Mater. Chem. C 3 (2015) 9948–9954, https://doi.org/10.1039/C5TC02155C.
[34] X.-L. Zhang, Z.-B. Liu, X. Zhao, X.-Q. Yan, X.-C. Li, J.-G. Tian, Optical limiting effect and ultrafast saturable absorption in a solid PMMA composite containing porphyrin-covalently functionalized multi-walled carbon nanotubes, Opt. Express 21 (2013) 25277, https://doi.org/10.1364/OE.21.025277.